Article

Multiscale stress deconcentration amplifies fatigue resistance of rubber

https://doi.org/10.1038/s41586-023-06782-2

Received: 23 December 2022

Accepted: 25 October 2023

Published online: 13 December 2023

Check for updates

Jason Steck[1,4], Junsoo Kim[1,3,4], Yakov Kutsovsky[2]✉ & Zhigang Suo[1]✉

Rubbers reinforced with rigid particles are used in high-volume applications, including tyres, dampers, belts and hoses[1]. Many applications require high modulus to resist excessive deformation and high fatigue threshold to resist crack growth under cyclic load. The particles are known to greatly increase modulus but not fatigue threshold. For example, adding carbon particles to natural rubber increases its modulus by one to two orders of magnitude[1–3], but its fatigue threshold, reinforced or not, has remained approximately 100 J m^{-2} for decades[4–7]. Here we amplify the fatigue threshold of particle-reinforced rubbers by multiscale stress deconcentration. We synthesize a rubber in which highly entangled long polymers strongly adhere with rigid particles. At a crack tip, stress deconcentrates across two length scales: first through polymers and then through particles. This rubber achieves a fatigue threshold of approximately 1,000 J m^{-2}. Mounts and grippers made of this rubber bear high loads and resist crack growth over repeated operation. Multiscale stress deconcentration expands the space of materials properties, opening doors to curtailing polymer pollution and building high-performance soft machines.

A filled rubber, also called particle-reinforced elastomer or composite for brevity, consists of a network of crosslinked polymer chains and a network of percolated rigid particles[2,3]. We form a polymer network in which polymer chains are long, and entanglements greatly outnumber crosslinks (Fig. 1a). Individual particles are much larger than individual polymer segments between entanglements. The polymer chains and particles interlink through strong bonds. As the volume fraction of particles increases, particles cluster and percolate (Fig. 1b). We use poly(ethyl acrylate) (PEA) and silica nanoparticles functionalized with 3-(trimethoxysilyl)propyl methacrylate (TPM) as a model system (Fig. 1c and Extended Data Fig. 1); Methods has a discussion on the model material, a discussion on the experimental crosslink density, and additional details on polymerization).

Our data will show that long polymers, clustered particles and strong polymer–particle adhesion synergize to amplify fatigue threshold. Consider a crack impinging on a polymer chain (Fig. 1a). We choose a polymer network with low friction between polymer chains such that stress deconcentrates over the entire polymer chain. Rupture of a single bond of the chain dissipates the energy stored in every bond along the chain[4]. Next, consider a crack impinging on a particle cluster (Fig. 1b). Strong polymer–particle adhesion transmits high stress from polymers to particles. Because the particles are rigid, stress deconcentrates over many particle–particle gaps in the cluster. Rupture of a single gap dissipates energy stored in many gaps in the cluster. Consequently, stress deconcentrates over two scales: polymers and particles. This multiscale stress deconcentration amplifies fatigue threshold (Methods discusses the mechanical model).

Our data will also show that entangled polymers and percolated particles synergize to amplify modulus (Extended Data Fig. 2). We choose a polymer with a low-entanglement molecular weight. In a network of long polymers, the polymer network is sparsely crosslinked, and dense entanglements set the modulus of the matrix. In turn, the modulus of the matrix scales the modulus of the composite. The scaling factor increases steeply when the particles percolate.

The requirements for high modulus differ from those for high fatigue threshold. High modulus requires densely entangled polymers and percolated particles. By contrast, high fatigue threshold requires long polymers and clustered particles, regardless of whether polymers are entangled or particles are percolated. To attain both high modulus and high fatigue threshold requires a network of densely entangled long polymers and a network of percolated particles. Also required are low friction between polymer chains and strong adhesion between polymers and particles.

Modulus

Each composite is synthesized with a crosslinker-to-monomer molar ratio, C, and a volume fraction of particles, F. We stretch the composites monotonically until rupture. The composites are initially transparent but become white under a large stretch (Fig. 2a). Upon unloading, the samples become transparent again. The slope of the stress–stretch curve at a small stretch defines the modulus. At fixed $C = 10^{-4}$, pure PEA has a modulus of 0.7 MPa, whereas the composites are much stiffer, achieving a modulus of 14 MPa at $F = 0.45$ (Fig. 2b). At fixed $F = 0.45$, the stress–stretch curves vary considerably with C (Fig. 2c). From the stress–stretch curves, we measure the properties at rupture, such as strength, maximum stretch and work of fracture, which show various trends with C and F (Extended Data Fig. 3). We also measure the storage

[1]John A. Paulson School of Engineering and Applied Science, Harvard University, Cambridge, MA, USA. [2]Office of Technology Development, Harvard University, Cambridge, MA, USA. [3]Present address: Department of Mechanical Engineering, Northwestern University, Evanston, IL, USA. [4]These authors contributed equally: Jason Steck, Junsoo Kim. ✉e-mail: yakov@materiax.ai; suo@seas.harvard.edu

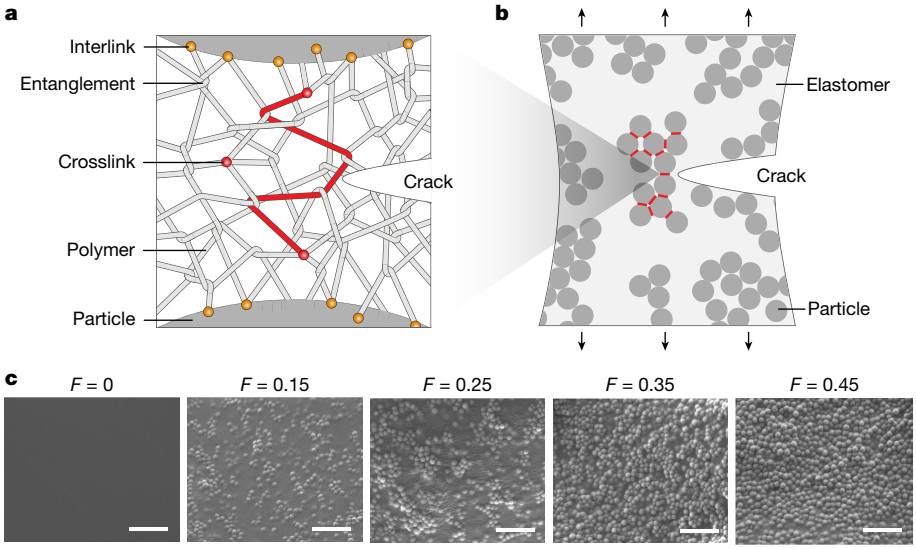

Fig. 1 | Fatigue threshold is amplified by synergy of long polymers, clustered particles and strong polymer–particle adhesion. a, When a crack impinges on a polymer chain, the rupture of a single bond on the chain dissipates the energy stored in all the bonds along the chain. **b**, When a crack impinges on a cluster of particles, the rupture of a single particle–particle gap dissipates the energy stored in many particle–particle gaps in the cluster. **c**, Scanning electron microscope (SEM) images of cross-sections of PEA elastomers reinforced with various volume fractions of silica nanoparticles, F, and a fixed crosslinker-to-monomer molar ratio, $C = 10^{-4}$. Scale bars, 1 µm.

modulus, loss modulus and loss tangent as functions of stretch rate by dynamic mechanical analysis (Supplementary Fig. 1).

For pure PEA, the modulus E plateaus when C is between 10^{-5} and $10^{-2.5}$ (Fig. 2d). Below $C \approx 10^{-5}$, the polymers do not form an elastic network. The plateau modulus originates from entanglements in the polymer network[8,9]. Uncrosslinked PEA chains have 82 monomers between two adjacent entanglements, corresponding to a rubbery plateau modulus of $E = 0.9$ MPa (ref. 10). This rubbery plateau modulus of uncrosslinked PEA is almost the same as the plateau modulus of the PEA networks measured in this work, indicating that entanglements set the modulus of pure PEA networks prepared with $10^{-5} < C < 10^{-2.5}$. Methods has further discussion on the entanglement density.

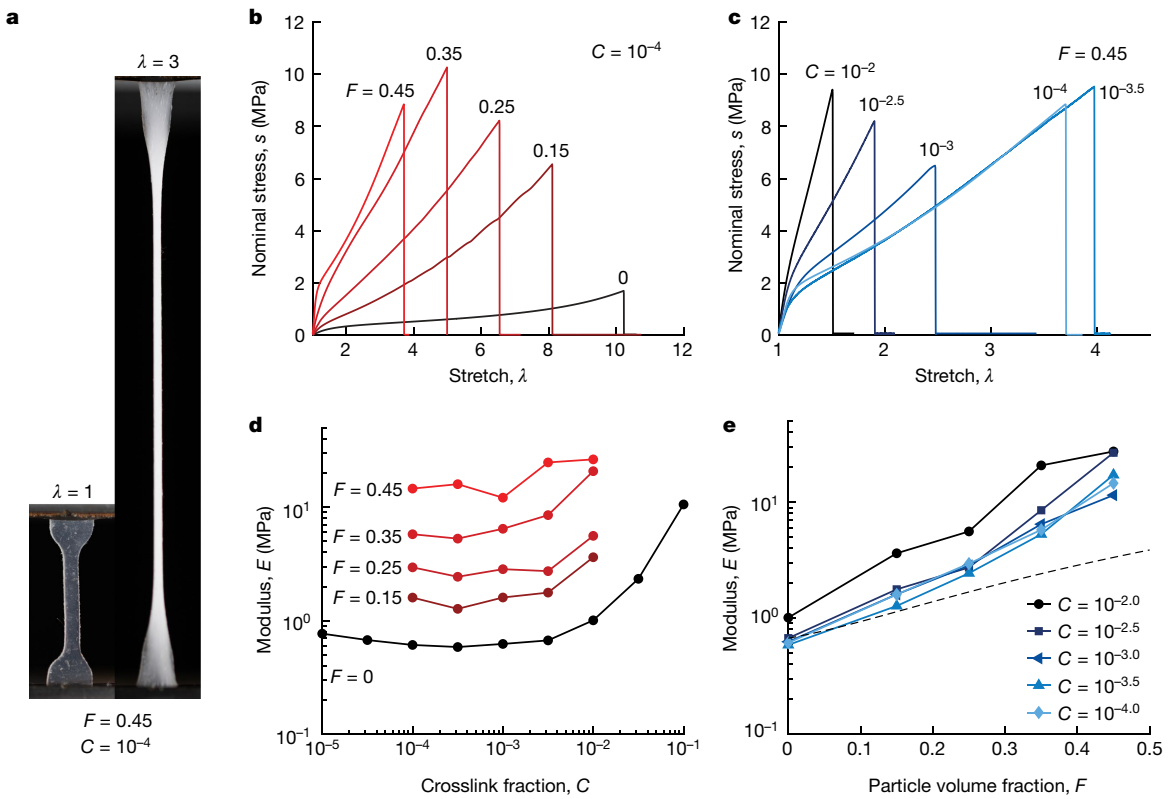

Fig. 2 | Composites under monotonic stretch. a, Photos of a composite with $F = 0.45$ and $C = 10^{-4}$ under uniaxial stretch. **b**, Stress–stretch curves of composites with $C = 10^{-4}$ and various F. **c**, Stress–stretch curves of composites with $F = 0.45$ and various C. **d**, Modulus E as a function of C for various F. **e**, E as a function of F for various C. The dashed line is the Guth–Gold solution for a composite of rigid spherical particles in a linear elastic matrix[11,12].

The composites show the same trends in C as pure PEA (Fig. 2d). The modulus plateaus when $C < 10^{-2.5}$, indicating that entanglements greatly outnumber crosslinks. Below $C \approx 10^{-4}$, the composites do not cure. Additionally, the modulus increases with F. We also plot E as a function of F (Fig. 2e). At all values of C, the modulus increases with F. When $C < 10^{-2.5}$, all lines collapse into one, indicating that E is not a function of C. When $C = 10^{-2}$, the line deviates from the collapsed lines because crosslinks outnumber entanglements. We compare our data with the Guth–Gold model for rigid spherical particles in a linear elastic matrix, $E(C, F) = E_0(C)(1 + 2.5F + 14.1F^2)$ (the dashed line in Fig. 2e)[11,12]. This solution follows the data approximately at low F but deviates greatly at high F. This deviation from the Guth–Gold model suggests that particles form a percolated network[2,13,14]. Indeed, deviation from the Guth–Gold model occurs near the percolation threshold of randomly dispersed impenetrable spheres, which percolate at $F = 0.20$ (ref. 15).

Inside the plateau, entanglements and particles synergize to increase the modulus. To characterize this synergy, we quantify the amplification of the modulus by the reinforcement ratio, $R = E/E_0$, where E is the modulus of the composite and E_0 is the modulus of pure PEA. The reinforcement ratio is a function of F but not of C (Extended Data Fig. 4). These observations indicate that the modulus of the composite takes the separable form $E(C, F) = E_0(C)R(F)$. Inside the plateau, the synergy between entanglements and particles is multiplicative: $E(F) = E_0R(F)$, where E_0 is set by entanglements and $R(F)$ increases steeply when particles percolate. Methods has further discussion on this scaling.

Cyclic stretch

We use rigid clamps to grip the two long edges of a rectangular membrane of a composite and cyclically stretch the membrane between one and a modest amplitude λ_{amp} (Supplementary Fig. 2). The stress–stretch curve changes with initial cycles but reaches a steady state after approximately 1,000 cycles (Fig. 3a). Using one membrane, we obtain the steady-state stress–stretch curves for various λ_{amp} (Fig. 3b). For each λ_{amp}, the loading and unloading curves are distinct, and the curves shift as λ_{amp} increases. In the steady state, the composite does not recover a stretch of one at zero stress. We also measure the steady-state stress–stretch curves for composites of various C and F (Supplementary Figs. 3 and 4). The steady-state modulus decreases with λ_{amp} when F is high but not when F is low (Extended Data Fig. 5a). This behaviour, called the Payne effect, further indicates that particles form a percolated network at high F (refs. 2,16). The steady-state modulus is insensitive to chain length when the polymers are highly entangled (Extended Data Fig. 5b). The steady-state hysteresis increases with F but varies negligibly with chain length (Extended Data Fig. 5c,d).

We study the recovery of the composite by applying sequences of 5,000 cycles of loading followed by 1 h of recovery. After one sequence, the composite almost recovers a stretch of one (Fig. 3c). The stress–stretch curve after this sequence is below the stress–stretch curve of the as-prepared sample, and the hysteresis loop is smaller. These observations suggest changes in microstructure, such as partial debonding between the particles and matrix, breaking polymer chains or formation of voids in the matrix. After a second sequence, the stress–stretch curve is nearly indistinguishable from that after the first sequence, indicating that the microstructure is stabilized. This is corroborated by the stress–stretch curves at various points throughout the sequences (Extended Data Fig. 6). Therefore, further changes in microstructure are negligible in the steady state, and both hysteresis and residual stretch indicate viscoelasticity. We note that although the filled rubber shows viscoelasticity, viscoelasticity does not increase fatigue threshold[4].

Multiscale stress deconcentration

We propose that stress deconcentration leads to high fatigue threshold through (1) covalent interlinks between particles and polymers; (2) long polymer chains; and (3) clustered particles (Fig. 1). We test this mechanism by modifying each component and observing their effects on fatigue crack growth. First, we prepare a composite with silica nanoparticles functionalized with trimethylsilyl (TMS) groups. Such particles do not form covalent interlinks with PEA polymers. The stress–stretch curves for such composites coincide with the stress–stretch curve of pure PEA, suggesting weak polymer–particle adhesion (Extended Data Fig. 7). We measure the crack growth per cycle dc/dN as a function of the amplitude of the energy release rate G (Fig. 3d and Extended Data Fig. 8). Without covalent interlinks, the fatigue threshold is the same as the polymer matrix, $G_{th} = 170$ J m^{-2}. By contrast, the composite with covalent interlinks has a fatigue threshold of $G_{th} = 420$ J m^{-2}. Strong interlinks enable clustered particles to carry high stress. Second, we measure the dc/dN–G curves of composites with $F = 0.45$ and various values of C (Fig. 3e). As C decreases, the fatigue threshold increases. We repeat this procedure for $F = 0$, $F = 0.15$, $F = 0.25$ and $F = 0.35$ and observe the same trends in C (Extended Data Fig. 9). Long polymer chains deconcentrate stress. Third, we measure the dc/dN–G curves of composites with $C = 10^{-4}$ and various values of F (Fig. 3f). Although the polymer matrix without particles has a fatigue threshold of $G_{th} = 170$ J m^{-2}, a composite of $F = 0.45$ has a fatigue threshold of $G_{th} = 1{,}020$ J m^{-2}. Clustered particles further deconcentrate stress. Taken together, these experiments support the mechanism of multiscale stress deconcentration.

The fatigue threshold is high when polymers are long and particles are concentrated (Fig. 3g). For all composites, the threshold scales approximately as $G_{th} \propto C^{-1/2}$, following the Lake–Thomas model[4]. For any given value of C, G_{th} increases with F. Even at $F = 0.15$, the fatigue threshold is about a factor of two higher than pure PEA. At $F = 0.15$, particles do not percolate but cluster (Fig. 1c). These observations are consistent with stress deconcentration over multiple thin layers of polymers between particles in a cluster (Fig. 1b; Methods discusses a mechanical model of multiscale stress deconcentration). It appears that the percolation threshold plays no special role in enhancing the fatigue threshold.

The crack growth per cycle dc/dN above the threshold quantifies the fatigue resistance under large loads. We plot the G required to cause $dc/dN = 5$ nm per one cycle (Fig. 3h). A crack growth rate of 5 nm per one cycle requires a load of $G = 20$ J m^{-2} for a short-chain polymer matrix without particles, but it requires a load of $G = 2{,}000$ J m^{-2} for a long-chain polymer matrix reinforced with a percolated network. This two orders of magnitude increase in fatigue resistance highlights the synergy of long polymer chains and clustered particles in deconcentrating stress.

For an application requiring elastic deformation over many cycles, the load-bearing capacity is mainly characterized by modulus and fatigue threshold. We compare these two properties for many elastomeric materials (Fig. 3i). The multiscale structure of entangled polymers and percolated particles enables the design of materials with properties that were previously unattainable. For the highest F and lowest C, we demonstrate a particle-reinforced elastomer with $G_{th} = 1{,}020$ J m^{-2} and $E = 14$ MPa.

Stiff and fatigue-resistant rubbers

Many applications require elastomeric materials of complex shapes and textured surfaces. Examples include gloves, textured belts, tyre treads and stamps for soft lithography. It has long been appreciated that particle-reinforced elastomers can be moulded into complex shapes because the particles are typically much smaller than the feature size of final shapes. Here, we make an aluminium mould of fine features by laser cutting and use the mould to cast a particle-reinforced elastomer (Fig. 4a). The moulded sample can undergo large deformation (Fig. 4b).

Many applications require materials to bear load over many cycles. Examples include vibration dampers, seals and o-rings[1]. For an elastic material, the load-bearing capacity is scaled by modulus, and a large

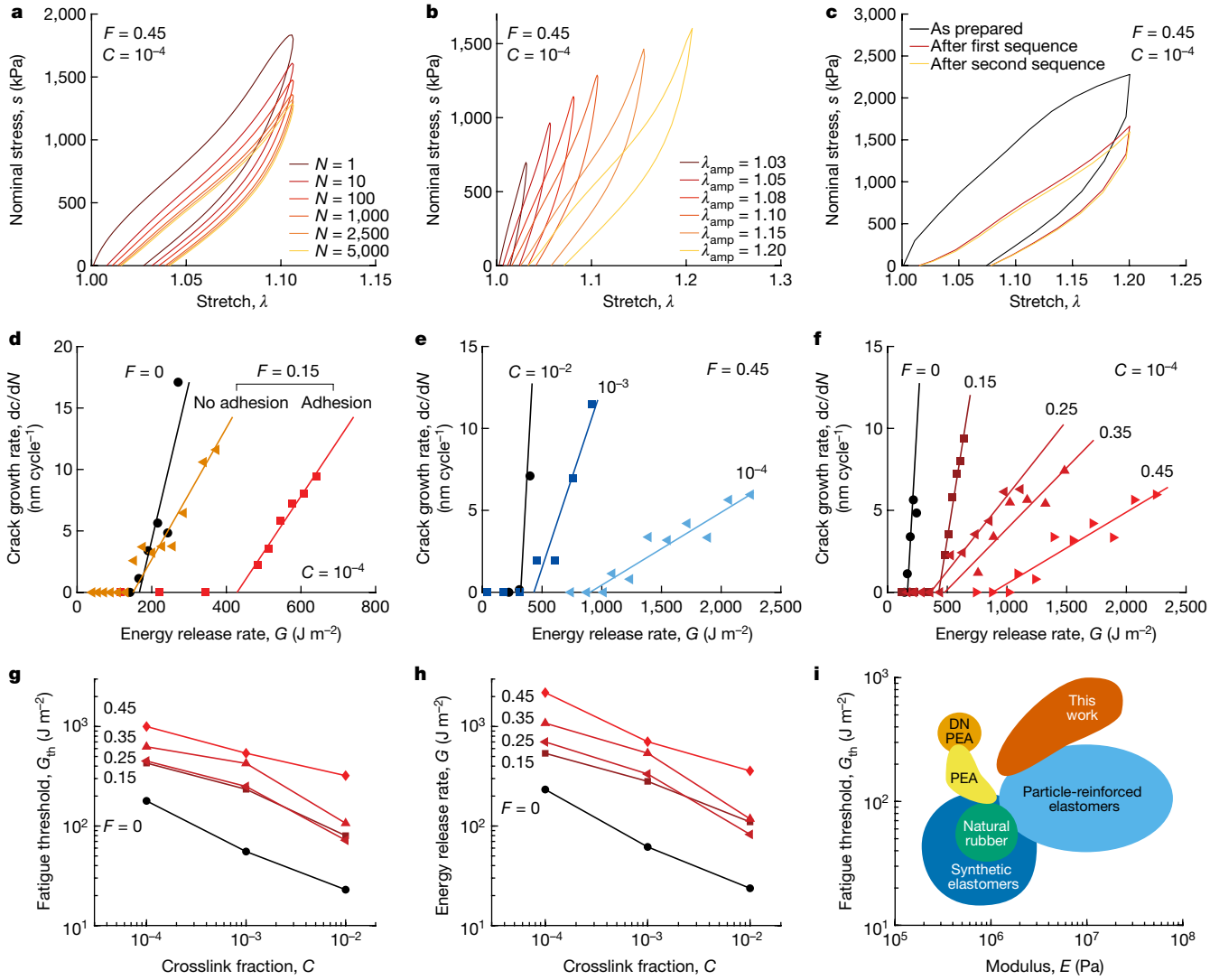

Fig. 3 | Composites under cyclic stretch. a, Stress–stretch curves under cyclic stretch. **b**, Stress–stretch curves at $N = 5{,}000$ for various stretch amplitudes λ_{amp}. **c**, The stress–stretch curve after a sequence of 5,000 cycles and 1 h of recovery is below that of the as-prepared composite. The stress–stretch curve does not change after a second sequence of 5,000 cycles and 1 h of recovery. **d**–**f**, Crack growth per cycle, dc/dN, is measured as a function of steady-state G for particles with and without covalent interlinks to polymers (**d**), various C (**e**) and various F (**f**). **g**, Fatigue threshold G_{th} as a function of C. **h**, G at dc/dN = 5 nm per one cycle as a function of C. **i**, Various crosslinked elastomers and double-network (DN) PEA compared on the plane of modulus and fatigue threshold[4,5,7,9,21,32].

number of cycles is enabled by high fatigue threshold. Here, we demonstrate the significance of both high modulus and high fatigue threshold using a cylindrical rubber mount with a crack (Fig. 4c). The crack opens when the mount is compressed. The mounts without particles are soft and either fracture at a low stress or deform excessively (Fig. 4d and Supplementary Video 1). The mount with particles and short chains is stiff but fractures at a modest load. By contrast, the mount with particles and long chains ($F = 0.45$ and $C = 10^{-4}$) is stiff and can support large loads repeatedly. For this mount, the crack does not advance appreciably after 33,000 cycles (Fig. 4e and Supplementary Video 2).

In soft robotics, materials need to bear loads over large and repeated displacements[17,18]. We demonstrate the significance of both high modulus and high fatigue threshold in a recent design of a compliant gripper (Fig. 4f)[19]. We choose this application because kirigami requires cuts by design, and grippers need to sustain cyclic deformation. The gripper is made using a square sheet with cuts parallel to a diagonal. When pulled along the other diagonal, the sheet buckles out of plane, gripping an object. Grippers with particles require larger forces to close than those without particles (Fig. 4g). We cyclically close and open the grippers. A gripper with $F = 0.45$ and $C = 10^{-2}$ fractures in only a few cycles (Supplementary Video 3). By contrast, a gripper with $F = 0.45$ and $C = 10^{-4}$ has negligible permanent deformation after $N = 350{,}000$ cycles, and the crack does not advance appreciably (Fig. 4h). Next, we use a gripper to grasp a sphere and measure the force required to lift the sphere (Extended Data Fig. 10 and Supplementary Video 4). A gripper with long polymer chains and percolated particles lifts a load six times that of a gripper made of pure PEA, and it maintains this lift force over many cycles. We discuss design considerations for kirigami grippers in Methods.

Discussion

For an elastomer in which entanglements greatly outnumber crosslinks, dense entanglements set high modulus, and sparse crosslinks set high fatigue threshold[9]. However, the density of entanglements is set by the entanglement molecular weight, limiting the modulus of the elastomer to approximately 1 MPa. A recent technique has enabled the synthesis of highly entangled elastomers from prepolymers, which

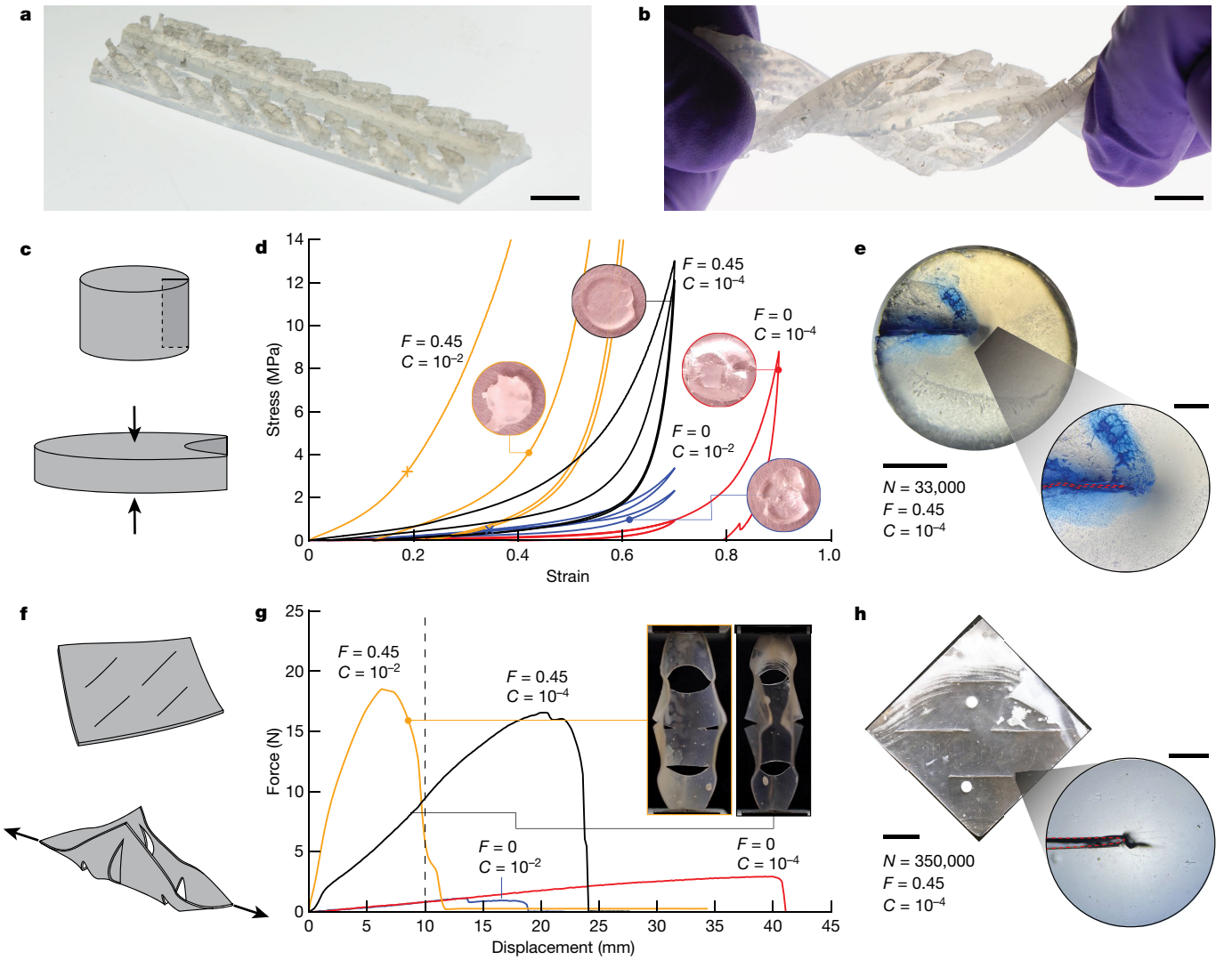

Fig. 4 | Applications of particle-reinforced elastomers with high stiffness and fatigue resistance. a, A particle-reinforced elastomer is moulded into a complex shape. **b**, The moulded sample can undergo large deformation. **c**, Schematic of a mount with a crack. The crack opens when the mount is compressed. **d**, The stress is measured as a function of strain for mounts of various C and F. Cyclic loadings of strain of 0.7 or 0.9 are applied. The point of fracture is marked on the plot. The insets are photographs of the samples at the marked points during the test. **e**, A mount of $C = 10^{-4}$ and $F = 0.45$ after $N = 33{,}000$ cycles. The inset is a magnified image of the sample, where the red dotted line shows the initial crack. **f**, Schematic of a gripper made of a flat sheet with cuts. When pulled, the sheet buckles out of plane. **g**, The force is measured as a function of displacement for grippers of various C and F. The dashed line indicates when the grippers are closed, and the insets show the grippers at this displacement. **h**, A gripper of $C = 10^{-4}$ and $F = 0.45$ after $N = 350{,}000$ cycles. The inset is a magnified image of the sample, where the red dotted line shows the initial crack. Scale bars, 1 cm (**a**,**b**,**e** (left),**h** (left)); 200 μm (**e**, right); 1 mm (**h**, right).

can be potentially used to make particle-reinforced elastomers of high fatigue resistance[20]. In an interpenetrating polymer network, the short-chain network provides high modulus, and the long-chain network provides high fatigue threshold[21–25]. However, the modulus achieved, 1–4 MPa, is still too low for many applications. Semicrystalline rubbers can have both high modulus and high fatigue threshold. For example, filled natural rubber crystallizes under strain, and when loaded under non-relaxing conditions, strain-induced crystallization greatly enhances the fatigue threshold[26,27]. However, strain-induced crystals melt when the stretch is relaxed each cycle, resulting in a fatigue threshold of approximately 100 J m^{-2}. Thermoplastic elastomers can achieve both high modulus and high fatigue threshold but suffer from creep[28,29]. Elastomers reinforced with fibres and fabrics can achieve both high modulus and threshold but are difficult to make into complex shapes and small features[30,31]. As demonstrated in this work, composites of entangled long polymer chains and percolated particles can also achieve both high modulus and threshold, as well as provide additional options in designing materials.

Whereas the effect of rigid particles on modulus has been appreciated for a century, the synergies of clustered particles and long polymer chains on fatigue threshold have not been identified before. Multiscale stress deconcentration is applicable to various types of rubber. Such materials can be explored in high-volume applications, such as tyres and belts, as well as emerging applications, such as soft robots and wearable devices. In addition to load-bearing capacity, particles can impart other functions, such as electrical conductivity, optical transparency, structural colour, magnetic actuation and high dielectric constants. High load-bearing capacity, along with diverse functions such as these, opens an enormous space for material design and applications.

Online content

Any methods, additional references, Nature Portfolio reporting summaries, source data, extended data, supplementary information, acknowledgements, peer review information; details of author contributions

and competing interests; and statements of data and code availability are available at https://doi.org/10.1038/s41586-023-06782-2.

1. GentA. N. *Engineering with Rubber: How to Design Rubber Components* (Carl Hanser, 2012).
2. Wang, M.-J. Effect of polymer-filler and filler-filler interactions on dynamic properties of filled vulcanizates. *Rubber Chem. Technol.* **71**, 520–589 (1998).
3. Heinrich, G. & Klüppel, M. Recent advances in the theory of filler networking in elastomers. *Adv. Polym. Sci.* **160**, 1–44 (2002).
4. Lake, G. J. & Thomas, A. G. The strength of highly elastic materials. *Proc. Royal Soc. Lond. Ser. Math. Phys. Sci.* **300**, 108–119 (1967).
5. Robertson, C. G., Stoček, R. & Mars, W. V. The fatigue threshold of rubber and its characterization using the cutting method. *Adv. Polym. Sci.* **286**, 57–84 (2020).
6. Gent, A. N., Lai, S.-M., Nah, C. & Wang, C. Viscoelastic effects in cutting and tearing rubber. *Rubber Chem. Technol.* **67**, 610–618 (1994).
7. Robertson, C. G., Stoček, R., Kipscholl, C. & Mars, W. V. Characterizing the intrinsic strength (fatigue threshold) of natural rubber/butadiene rubber blends. *Tire Sci. Technol.* **47**, 292–307 (2019).
8. Rubinstein, M. & Colby, R. H. *Polymer Physics* (Oxford Univ. Press, 2003).
9. Kim, J., Zhang, G., Shi, M. & Suo, Z. Fracture, fatigue, and friction of polymers in which entanglements greatly outnumber cross-links. *Science* **374**, 212–216 (2021).
10. Andreozzi, L., Castelvetro, V., Faetti, M., Giordano, M. & Zulli, F. Rheological and thermal properties of narrow distribution poly(ethyl acrylate)s. *Macromolecules* **39**, 1880–1889 (2006).
11. Guth, E. & Gold, O. On the hydrodynamical theory of the viscosity of suspensions. *Phys. Rev.* **533**, 322 (1938).
12. Guth, E. Theory of filler reinforcement. *Rubber Chem. Technol.* **18**, 596–604 (1945).
13. Bergström, J. S. & Boyce, M. C. Mechanical behavior of particle filled elastomers. *Rubber Chem. Technol.* **72**, 633–656 (1999).
14. Sotta, P. et al. Nonentropic reinforcement in elastomer nanocomposites. *Macromolecules* **50**, 6314–6322 (2017).
15. Torquato, S. *Random Heterogeneous Materials* (Springer, 2002).
16. Payne, A. R. The dynamic properties of carbon black-loaded natural rubber vulcanizates. Part I. *J. Appl. Polym. Sci.* **6**, 57–63 (1962).
17. Laschi, C., Mazzolai, B. & Cianchetti, M. Soft robotics: technologies and systems pushing the boundaries of robot abilities. *Sci. Robot.* **1**, eaah3690 (2016).
18. Hawkes, E. W., Majidi, C. & Tolley, M. T. Hard questions for soft robotics. *Sci. Robot.* **6**, eabg6049 (2021).
19. Yang, Y., Vella, K. & Holmes, D. P. Grasping with kirigami shells. *Sci. Robot.* **6**, eabd6426 (2021).
20. Hu, P., Madsen, J. & Skov, A. L. One reaction to make highly stretchable or extremely soft silicone elastomers from easily available materials. *Nat. Comm.* **13**, 370 (2022).
21. Sanoja, G. E. et al. Why is mechanical fatigue different from toughness in elastomers? The role of damage by polymer chain scission. *Sci. Adv.* **7**, eabg9410 (2021).
22. Zhang, W. et al. Fatigue of double-network hydrogels. *Eng. Fract. Mech.* **187**, 74–93 (2018).
23. Ducrot, E., Chen, Y., Bulters, M., Sijbesma, R. P. & Creton, C. Toughening elastomers with sacrificial bonds and watching them break. *Science* **344**, 186–189 (2014).
24. Gong, J. P., Katsuyama, Y., Kurokawa, T. & Osada, Y. Double-network hydrogels with extremely high mechanical strength. *Adv. Mater.* **15**, 1155–1158 (2003).
25. Zhou, Y. et al. Flaw-sensitivity of a tough hydrogel under monotonic and cyclic loads. *J. Mech. Phys. Solids* **153**, 104483 (2021).
26. Persson, B. N. J., Albohr, O., Heinrich, G. & Ueba, H. Crack propagation in rubber-like materials. *J. Phys. Condens. Matter* **17**, R1071 (2005).
27. Creton, C. & Ciccotti, M. Fracture and adhesion of soft materials: a review. *Rep. Prog. Phys.* **79**, 046601 (2016).
28. Scetta, G. et al. Self-organization at the crack tip of fatigue-resistant thermoplastic polyurethane elastomers. *Macromolecules* **54**, 8726–8737 (2021).
29. Scetta, G. et al. Strain induced strengthening of soft thermoplastic polyurethanes under cyclic deformation. *J. Polym. Sci.* **59**, 685–696 (2021).
30. Wang, Z. et al. Stretchable materials of high toughness and low hysteresis. *Proc. Natl Acad. Sci. USA* **116**, 5967–5972 (2019).
31. Cui, W. et al. Fiber-reinforced viscoelastomers show extraordinary crack resistance that exceeds metals. *Adv. Mater.* **32**, 1907180 (2020).
32. Fleck, N. A., Kang, K. J. & Ashby, M. F. The cyclic properties of engineering materials. *Acta Metall. Mater.* **42**, 365–381 (1994).

Methods

Model material

PEA is selected to meet three requirements. PEA can be made into long chains, has a low-entanglement molecular weight and has low interchain friction. The silica nanoparticles are 110 nm diameter spheres (Supplementary Fig. 5), and their surfaces are functionalized with TPM. Ethyl acrylate (EA) monomer is a liquid, in which we mix small amounts of crosslinker and initiator, as well as silica nanoparticles. We fix the initiator-to-crosslinker molar ratio to 0.4 and vary the crosslinker-to-monomer molar ratio C and the volume fraction of silica particles F. When the mixture is exposed to ultraviolet (UV) light, a polymer network is formed by free radical polymerization. Most monomers polymerize, and most polymers crosslink into the polymer network (Supplementary Fig. 6). Some of the monomers react with TPM groups on the surfaces of the particles, forming covalent interlinks between the polymer network and silica particles (Extended Data Fig. 1). On the surfaces of the silica particles, the number density of TPM groups is 2.7 nm^{-2}, which is measured by the manufacturer. Functionalized nanoparticles have long been used as reinforcing fillers in industrial applications[1,2]. Additionally, TPM-functionalized silica nanoparticles have been used as reinforcing fillers in PEA elastomers[33,34], but these works used polymer chains much shorter than reported here and did not report fatigue threshold. Although the precursor mixtures are opaque and white (Supplementary Fig. 7), the composites are transparent (Supplementary Fig. 8). These observations are consistent with the refractive indices: 1.407 for EA monomer, 1.467 for PEA (ref. 35) and 1.475 for silica nanoparticles[36].

Mechanics of multiscale stress deconcentration

Consider an elastomer filled with rigid particles of volume fraction F. A crack in the composite impinges both on polymer chains (Fig. 1a) and on clusters of particles (Fig. 1b). Near the crack tip, stress deconcentrates across both long polymer chains and clustered particles.

First, consider a crack growing in the elastomer network (Fig. 1a). Before a polymer chain breaks, stress is deconcentrated over the entire length of the chain. Rupture of a single bond along the chain dissipates energy stored in every bond along the chain. According to Lake and Thomas[4], the fatigue threshold of the polymer matrix, $G_{th,m}$, is the covalent energy per unit area of one layer of polymer chains.

Next, consider a crack growing in a particle-filled elastomer (Fig. 1b). Particles cluster and percolate. Within a cluster, the thickness of the gap between two particles is small, comparable with a layer of polymer chains. The fatigue threshold of each gap is $G_{th,m}$. Because the particles are rigid compared with the polymer matrix, the stress to rupture one gap is deconcentrated to several other gaps in the particle cluster. When the crack grows through one gap, the energy stored in many gaps is released. The fatigue threshold of a cluster of particles is $N_g G_{th,m}$, where N_g is the number of gaps in the cluster that participate in stress deconcentration.

By rule of mixture, write the threshold of the composite as $G_{th} = FN_gG_{th,m} + (1 - F)G_{th,m}$. Like modulus, the fatigue threshold takes a separable form $G_{th}(C, F) = G_{th,m}(C)R_{th}(F)$, where the particles amplify the fatigue threshold by a factor

$$R_{th}(F) = F(N_g - 1) + 1. \quad (1)$$

The threshold of the matrix scales the threshold of the composite, $G_{th} \propto G_{th,m}$. Therefore, the threshold of the composite will follow the scaling of the Lake–Thomas model, $G_{th} \propto C^{-1/2}$. Long polymer chains and clustered particles synergize to increase the threshold of the composite.

We plot the threshold reinforcement ratio R_{th} at various values of F and C (Supplementary Fig. 9a). R_{th} is not sensitive to changes in C, as changing C by 100 times changes R_{th} by at most a factor of three. Consistent with equation (1), we write the fatigue threshold of the composite in a separable form: $G_{th} = G_{th,m}(C)R_{th}(F)$. Using equation (1), we estimate the number of gaps N_g that participate in stress deconcentration (Supplementary Fig. 9b). Unlike R_{th}, N_g does not vary substantially with F. These observations show that R_{th} is more strongly a function of the volume fraction of particles than N_g. Across all C and F, we measure an average value of $N_g = 13.6$. We note that if the adhesion between particles and polymers is not strong, the threshold of the composite is not increased with particle reinforcement (Fig. 3d). Without strong adhesion, stress is not deconcentrated from the scale of a polymer chain to that of clustered particles.

Experimental crosslink density

The experimental crosslink density is defined by the experiment used to measure it. For a polymer network with negligible entanglements, the elastic modulus is related to the crosslink density as $E = 3\rho N_{Av}kT/M_s$, where ρ is the density, N_{Av} is Avogadro's number, kT is the temperature in units of energy and M_s is the molecular weight of polymer strands between crosslinks (ref. 8, equation 7.31). Therefore, the experimental crosslink density can be estimated from the elastic modulus. For example, at $F = 0$ and $C = 10^{-2.5}$, the modulus is 0.7 MPa. This modulus gives the molecular weight of 12,070 g mol^{-1} or 109 monomers per chain. In the manuscript, we estimated the length of the polymer chain as $1/(2C) = 158$ monomers, which is similar to the crosslink density estimated by the modulus.

For a highly entangled polymer network, by contrast, the elastic modulus is related to the entanglement density as $E = 3\rho kT/M_e$, where M_e is the molecular weight of polymer strands between entanglements (ref. 8, equation 7.47). Therefore, the elastic modulus does not provide experimental crosslink density. Instead, the crosslink density can be related to the fatigue threshold for a highly entangled polymer network. The Lake–Thomas model relates the fatigue threshold to the crosslink density as $G_0 = \alpha l n^{1/2} J V^{-1}$, where α is a prefactor of order of unity, l is the length of each monomer unit, n is the number of monomer units in a polymer chain, J is the C–C bond energy and V is the volume of each monomer unit[4]. Therefore, the experimental crosslink density of a highly entangled polymer network can be calculated by scaling ($G_0 \propto n^{1/2}$). This scaling corresponds to our data ($G_0 \propto C^{-1/2}$) (Fig. 3g) as $n \propto C^{-1}$. For example, the fatigue thresholds of pure PEA elastomers at $C = 10^{-2}$ and $C = 10^{-4}$ are approximately 20 J m^{-2} and approximately 200 J m^{-2}, respectively. Therefore, the values of n are expected to be different by 100 times. As n at $C = 10^{-2}$ is estimated as approximately 100 monomers per chain from the modulus, n at $C = 10^{-4}$ is approximately 10,000 monomers per chain.

Additional discussion on polymerization

Adhesion between particles and polymer matrix. The reaction between methacrylate groups on the particles and acrylate monomers is faster than the reaction between acrylate monomers[37]. In principle, all the methacrylate groups on the particles could be consumed without coupling the particles to polymer chains in the matrix. However, our experiments indicate that particles do adhere to the matrix. PEA filled with TPM-functionalized silica particles has a much higher modulus and fatigue threshold than PEA filled with TMS-functionalized silica particles (Fig. 3d and Extended Data Fig. 7). The TPM-functionalized particles and the PEA matrix can adhere by two mechanisms. First, TPM copolymerizes with PEA in the matrix such that covalent bonds form between particles and the polymer matrix. Second, a PEA loop anchored on a particle can form trapped entanglements with PEA chains in the matrix. Both types of adhesion are illustrated in Fig. 1a.

Side reaction. Radical polymerization of polyacrylates, such as PEA, is accompanied by side reactions that cause polymer chains to branch[38]. Like crosslinks, branches reduce the chain length, and branches can even form a network in the absence of crosslinkers. As an additional experiment, we prepare pure PEA without crosslinker, $C = 0$, but with

initiator, $I = 4 \times 10^{-5}$. This sample dissolves in propylene carbonate, indicating that a network did not form. By contrast, pure PEA forms a network at $C = 1 \times 10^{-4}$ and $I = 4 \times 10^{-5}$, and it even forms a network at much lower concentrations of crosslinker and initiator, $C = 1 \times 10^{-6}$ and $I = 4 \times 10^{-7}$ (ref. 9). These observations indicate that under the conditions of this work, $I/C = 0.4$, side reactions occur less frequently than reactions with crosslinkers. We surmise that branching is negligible in our samples because they are prepared with $I < C$ and with unusually low concentrations of initiator.

Initiator concentration. The molar ratio of initiator to crosslinker was set to $I/C = 0.4$ for all samples. This value of I/C was chosen based on the following considerations. When initiators are triggered, they form radicals. The radicals drive polymerization by reacting with either monomers or crosslinkers. Assume that polymerization is terminated by recombination and ignore side reactions. After polymerization, polymer strands connect two crosslinks, one initiator and one crosslink, or two initiators. These three types of polymer strands are often called network chain, dangling chain and linear chain, respectively. Only network chains carry load when the polymer network is stretched.

When I is much lower than C, the number of dangling chains and linear chains is negligible compared with the number of network chains. By contrast, when I is much higher than C, dangling chains and linear chains can outnumber network chains, resulting in a poor polymer network where most of the polymer strands do not carry load. Therefore, to produce a polymer network in which most polymer strands carry load, I should be low enough compared with C. Our previous work showed that PEA prepared with $I/C = 10$ creeps when subject to a constant load[9]. In this work, we set $I/C = 0.4$ for all samples.

Furthermore, if I is too low, then polymerization will be quenched by oxygen dissolved in the precursor, and the sample will not cure. As C is reduced, it becomes increasingly difficult to satisfy $I/C = 0.4$ while maintaining an I high enough to cure the sample. In our experiments, composites with $C < 10^{-4}$ do not cure.

Entanglement density

The molar ratio C sets the chain length. For PEA, one crosslink connects four chains, and one chain connects two crosslinks so that the average number of monomers between two adjacent crosslinks is estimated as $1/(2C)$. When $C = 10^{-4}$, there are approximately 5,000 monomers between two adjacent crosslinks, much greater than the number of monomers between two adjacent entanglements, 82. Therefore, the modulus is set by entanglements. By contrast, when $C > 10^{-2}$, the chains are shorter than the spacing between entanglements. In this case, the modulus is set by crosslinks, and E is linear in C (ref. 8).

Discussion on the scaling of modulus

We interpret the scaling of the modulus, $E(C, F) = E_0(C)R(F)$, as follows. The composite has three microscopic length scales: the diameter of individual particles ($D \approx 110$ nm), the average distance between neighbouring entanglements ($\xi \approx 10$ nm) and the thickness of a layer of polymer of reduced mobility near the particles ($\varepsilon \approx 2$ nm) (ref. 39). In the limit of $D \gg \xi, \varepsilon$, the composite can be treated as rigid particles in a continuum matrix, where ξ is contained in the modulus of the matrix E_0, and ε modifies D negligibly. Dimensional analysis indicates that the only remaining length scale, D, does not affect the modulus of the composite. Consequently, the modulus of the composite is proportional to the modulus of the matrix, $E = E_0R$, which corresponds to our observation. The scaling factor R depends on the volume fraction of particles F and their arrangement, such as when the particles form a percolated network. We note that, although modulus increases steeply when particles percolate, percolation theory by itself does not explain how entangled polymers and percolated particles synergize to increase modulus.

Design of mechanical properties of kirigami grippers

In designing elastomeric kirigami grippers, one may consider the following.

Stretchability. The displacement required to close the gripper is approximately 10 mm, and excess stretchability is redundant. As described in ref. 19, the actuation displacement is a geometric quantity unrelated to the mechanical properties of the material, assuming that fracture does not occur.

Fatigue resistance. The higher the fatigue resistance, the better the durability and reliability. The fatigue resistance increases with F and decreases with C.

Stiffness. The gripping force and the lift force scale with the stiffness. The required force will differ depending on the application. Provided that low C provides high fatigue resistance while the stiffness is maintained by entanglements, one can tune F to design the stiffness. For example, varying F from 0 to 0.45 at $C = 10^{-4}$ varies the modulus from 0.6 to 14 MPa. Although reducing F decreases the fatigue resistance, the threshold can still be relatively high with low C. Furthermore, the energy release rate G at a fixed strain scales with modulus, making fatigue threshold requirements for stiff materials greater than for soft materials. For example, G scales with E for a linear elastic material at fixed applied strain.

Structural design. Elastomers of high fatigue resistance, high stiffness and stretchability open doors to new possibilities in the design of kirigami structures. For example, recent works have developed elastomeric kirigami structures that can be actuated by nonmechanical means, such as magnets or temperature[19,40]. We look forward to seeing new kirigami applications.

Synthesis of composites

EA (E9706), tricyclo[5.2.1.$0^{2,6}$]decanedimethanol diacrylate (TDDA; 496669), 2-hydroxy-2-methylpropiophenone (Irgacure 1173; 405655) and *N,N*-dimethylformamide (DMF; 227056) are used as monomer, crosslinker, photo-initiator and solvent, respectively. These reagents were purchased from Sigma Aldrich and used as received. Silica nanoparticles functionalized with TPM of areal density 2.7 molecules per 1 nm^2 were used as reinforcing particles (Cabot Corporation; Silica A), and silica nanoparticles functionalized with TMS groups were used as non-adhesive particles (Cabot Corporation; Silica B). From the diameter of the nanoparticles, the specific area is calculated as 26 $m^2\ g^{-1}$. Both types of particles were supplied by Cabot Corporation as a powder and were used as received. We made solutions of Irgacure 1173 and TDDA with DMF. The concentration of TDDA was varied, depending on the amount required for the composite, such that the concentration of DMF in the precursor solution was less than 5 vol%. The molar ratio of Irgacure 1173 to TDDA was set to $I/C = 0.4$ for all samples. Moulds consisted of glass plates (8476K15; McMaster) separated by a silicone sheet (1460N11; McMaster, thickness = 0.79 mm). Silicone mould release (CRC; no. 03300) was sprayed on the surfaces of the glass plates and allowed to dry for 5 min before use.

A precursor solution for a composite was prepared by first mixing EA and silica nanoparticles. Silica nanoparticles were first weighed in a nanoparticle fume hood and poured into a conical tube. Then, the conical tube was sealed, placed in an airtight plastic bag and moved to a chemical fume hood, and then, EA was added to the tube. The volume of EA added to the tube was calculated from the target particle volume fraction, F. We calculate the mass of silica nanoparticles as $m_{silica} = F\rho_{silica}V_{EA}$, where V_{EA} is the volume of EA and $\rho_{silica} = 2.20$ g cm^{-3} is the density of silica glass. This neglects the volume of the crosslinker and initiator, and it assumes that the volume of EA does not change upon polymerization. For composites with $C = 10^{-2}$, the volume change

upon adding crosslinker and initiator is approximately 10%, whereas that for $C = 10^{-4}$ is approximately 0.1%. The mixture of EA and silica nanoparticles was then stirred in a vortex mixer at 3,000 rpm for 1 min and sonicated at room temperature for 3 min. The particles incorporate well with the monomer for F used in the study. For F greater than 0.45, the particles did not completely incorporate with the monomer. Mixtures of $F = 0.15$ and 0.25 had viscosities similar to the monomer. At $F = 0.35$, the mixture was a liquid with a higher viscosity than the monomer. At $F = 0.45$, the mixture was a plastic liquid. Afterward, the crosslinker and initiator solutions were added to the mixture, where the concentration of crosslinker was set by the molar ratio of crosslinker to monomer, C. The precursor solution was then vortexed again at 3,000 rpm for 1 min. The precursor solution was then poured into a mould and sealed with a glass plate. Binder clips were attached along the perimeter of the mould. The mould was placed in a plastic bag (Minigrip Redline; VWR) filled with nitrogen gas, and excess gas was pressed out of the bag before it was sealed. The mould was then irradiated with a UV lamp (8337K11; McMaster) for at least 12 h with an intensity of 1.5 mW cm^{-2}. After curing, the sample was removed from the mould, the mass of the as-prepared sample was measured, and the sample was placed for 1 day in a fume hood to allow unreacted monomers and DMF to evaporate. The thickness of all samples was 0.8 mm.

Sol and gel fraction

We prepare a PEA elastomer of $F = 0$ and $C = 10^{-4}$. We measure the mass of the sample before curing, after curing and after degassing in air for 48 h. We then submerge the degassed sample in a reservoir of ethyl acetate solvent[41,42]. The sample swells in the solvent, where the mass fraction of polymer in the fully swollen sample is 11.8 wt%. While submerged in the solvent, uncrosslinked polymers and monomers diffuse out of the elastomer and into the reservoir of ethyl acetate. After 1 week, we remove the elastomer from the solvent and allow the solvent in the sample to evaporate in air for 3 days. We measure the mass of the washed sample. The gel fraction is calculated from the mass of the washed sample divided by the mass of the as-prepared sample, and the sol fraction is calculated as one minus the gel fraction. Most polymer chains are crosslinked into a polymer network (Supplementary Fig. 6).

Imaging

Images and videos of samples at large length scales were obtained using a digital camera (Canon; EOS 50D). SEM images were taken using a Zeiss Ultra Plus FESEM. Before SEM imaging, the samples were cut with scissors, mounted on an SEM stub with carbon tape such that the cross-section was facing up and coated with a 5 nm thick Pt/Pd layer using a metal sputter coater (208HR; Cressington Scientific Instruments). All SEM images were taken of the Pt/Pd-coated cross-section.

Monotonic mechanical tests

A sample of the composite was cut into a dog-bone shape with a die (ISO 37-2). The sample was then gripped in a tensile tester (Instron; 5966) with screw action grips (Instron) and stretched at a rate of 0.2 s^{-1} until rupture. The stretch λ was calculated as the deformed length divided by the undeformed length, and the stress s was calculated as the applied force divided by the cross-sectional area of the undeformed sample. The modulus E was calculated as the slope of the stress–stretch curve at a small stretch (less than 0.05). Rupture occurred at stretch λ_{max}. The nominal strength s_{max} was calculated as the stress when the sample ruptured. The true strength σ_{max} was calculated as the product $\lambda_{max}s_{max}$. The work of fracture W_f was calculated by numerically integrating the stress–stretch curve until rupture.

Cyclic mechanical tests

For all cyclic mechanical tests, we used the pure shear geometry. A sample of composite was cut into a rectangle of dimensions 60 × 30 mm. An adhesion primer (Loctite 7701) was applied to both sides of the sample and to four glass microscope slides (Globe Scientific Inc.; 1321) and allowed to evaporate for 3 min in a fume hood. Then, the sample was glued to the slides with a cyanoacrylate adhesive (Krazy Glue) such that the height of the unbonded portion was 10 mm. Stress–stretch curves in cyclic loading were obtained by stretching uncracked pure shear samples in the Instron tensile tester. All samples were stretched at a stretch rate of 0.2 s^{-1}. The samples were gripped in the tensile tester using screw action grips. To prevent cracking of the microscope slides, six silicone sheets were used to shield the slides from each other and the grips of the tester.

Several quantities were calculated from the cyclic stress–stretch curves. The modulus E in cyclic loading (for example, Extended Data Fig. 5) was calculated as three quarters the slope of the stress–stretch curve when the stress was zero. The hysteresis ratio H (for example, Extended Data Fig. 5) was calculated as the numerical integration of the positive portion of the unloading stress–stretch curve divided by that of the loading curve.

Dynamic mechanical analysis tests were performed using a dynamic mechanical analysis instrument (Mettler Toledo) and the tension geometry. The stretch amplitude was fixed at $\lambda = 0.01$, and the temperature was 25 °C.

Crack growth measurements

The driving force for crack growth is the energy release rate, G. For the pure shear geometry, G is calculated by multiplying the sample height, H, by the area under the stress–stretch curve of an equivalent sample without a crack[43]. Stress–stretch curves of pure shear samples without cracks were obtained as described in the previous section. Because the stress–stretch curves vary with cycles, we calculate G from the stress–stretch curves in the steady state (for example, the curves in Fig. 3b). Furthermore, because the stress–stretch curves in the steady state vary with λ_{amp}, we calculate G for each λ_{amp}. For one sample, this produces G for discrete values of λ_{amp}. We obtain an equation for G as a function of the applied stretch λ_{amp} by a quadratic least-squares regression. We repeat this procedure for samples of various combinations of C and F (Supplementary Figs. 3, 4 and 10). Every combination of C and F has a corresponding equation for G as a function of λ_{amp}.

To measure crack growth, a pure shear sample was prepared with a crack of length $c = 2$ cm (Supplementary Fig. 2b). The crack was cut from a free edge of the sample with scissors, and the tip of the crack was marked with a marker (Sharpie). The sample was then placed in a fatigue tester and stretched to a peak stretch of λ_{amp} for 50,000 cycles. The stretch rate was 0.2 s^{-1}, and the force was not recorded during the test. The energy release rate corresponding to the applied stretch λ_{amp} was then calculated using the sample's corresponding equation for G. After each test, the crack was observed using an optical microscope (Omax) with a resolution of approximately 10 μm, and a photograph was taken through the lens of the microscope. The crack growth was measured by comparing the crack length in each photo (Extended Data Fig. 10). The crack growth per cycle, dc/dN, was calculated as the crack growth divided by the number of cycles. For 50,000 cycles, the resolution in dc/dN is 0.2 nm per 1 cycle. For one sample, the crack growth per cycle dc/dN was measured for many energy release rates G. dc/dN varies with the applied G, and crack growth is not observed when G is below the fatigue threshold, G_{th}.

Differential scanning calorimetry

We characterized the composites with a differential scanning calorimeter (TA Discover differential scanning calorimeter 250). Using the differential scanning calorimeter, samples were heated to 75 °C, cooled to −75 °C and heated to 75 °C while measuring the heat flow through the samples. The heat flow normalized by the mass of the sample is plotted as a function of temperature for various composites (Supplementary Fig. 11).

Moulding demonstration

A stencil was cut from an aluminium sheet (5052 Aluminium; SendCutSend). The stencil was 3.2 mm thick. A mould was constructed by

gluing the metal stencil to a glass plate along the perimeter of the metal stencil with hot glue. Two silicone sheets (1460N11; McMaster) were cut and placed on the free face of the metal stencil such that there was a 0.5 cm wide silicone frame along the outer edge of the mould. The two sheets were identical and stacked on top of each other, making the border 1.6 mm tall. Mould release was sprayed in the mould and allowed to dry. A precursor solution was then poured into the mould and sealed with a glass plate. The mould was then compressed with binder clips, sealed in a plastic bag filled with nitrogen gas and irradiated with the UV lamp for at least 12 h.

Mount

A mount was cut from a sheet of composite (thickness of approximately 3 mm) using a pin punch (diameter of approximately 3 mm). The geometry of the mount is shown in Fig. 4c, where the length of the cut is approximately one quarter of the diameter of the mount. The mount is placed between two rigid plates as shown in Supplementary Fig. 12. The top plate is made of a transparent acrylic plate, and the top of the frame is clamped to the upper substrate of the Instron. During compression, the force and displacement applied by the Instron transmit through the frame to the sample, while a digital camera (Handheld Digital Microscope Pro; Celestron) records the deformation of the mount from above. The stress is calculated as the applied force divided by the undeformed area, and the strain is calculated as the applied displacement divided by the undeformed height. The diameter and height are measured for each mount.

Cyclic compression is applied using linear loading and unloading curves, a strain amplitude of 0.7 and a velocity of 0.02 mm s^{-1}. The deformation was recorded using the digital camera (Supplementary Video 1). For the mount with $F = 0$ and $C = 10^{-4}$, a strain amplitude of 0.9 is applied at the last cycle.

In fatigue loading, the same setup was used, except that the minimum strain was 0.3 so that the mount does not move during the test and the velocity was set to 2 mm s^{-1}. The crack growth was measured by using a microscope (Fig. 4e).

Compliant gripper

A gripper was cut from a film of composite (thickness = 0.8 mm) using a razor blade. The geometry of the gripper is shown in Fig. 4f, where the side length of the square was 4 cm and all cuts were 1 cm long. All force–displacement curves were obtained using the Instron. For the actuation force–displacement curves (for example, Fig. 4g), the gripper was mounted along the diagonal with the screw action grips and pulled at a velocity of 2 mm s^{-1} until rupture. In fatigue loading, the same setup was used, except the maximum displacement was set to 10 mm. A 25 mm diameter sphere mounted on a 30 mm long post was three-dimensionally printed. The lift force was measured by mounting the post in the Instron, mounting the gripper in a fatigue tester, actuating the gripper with a 10 mm displacement to grasp the sphere and pulling the sphere out of the gripper at a velocity of 5 mm s^{-1}.

Fatigue tester

To measure the crack growth per cycle dc/dN as a function of energy release rate G for various values of F and C, we built multiple fatigue testers (Supplementary Fig. 13). Each tester can apply cyclic loading of a fixed displacement and velocity. The velocity is 2 mm s^{-1} for all samples. The linear motor (300 mm SFU1605 linear guide rail with NEMA17 stepper motor; SainSmart), stepper motor driver (DM542T; Stepperonline) and controller (Arduino Uno) were purchased from Amazon. The linear motor was mounted at the homemade jig made of acrylic sheets as shown in Supplementary Fig. 13.

Data availability

The cyclic stress–stretch curves and energy release rates as a function of stretch for all synthesis conditions, as well as the Arduino code for the fatigue testers, are provided in the Supplementary Information. Raw monotonic and cyclic stress–stretch curves are available from the corresponding authors on request.

33. Berriot, J., Martin, F., Montes, H., Monnerie, L. & Sotta, P. Reinforcement of model filled elastomers: characterization of the cross-linking density at the filler–elastomer interface by 1H NMR measurements. *Polymer* **44**, 1437–1447 (2003).
34. Berriot, J. et al. Reinforcement of model filled elastomers: synthesis and characterization of the dispersion state by SANS measurements. *Polymer* **44**, 4909–4919 (2003).
35. LideD. R. *CRC Handbook of Chemistry and Physics: A Ready-Reference Book of Chemical and Physical Data* (CRC, 2008).
36. Khlebtsov, B. N., Khanadeev, V. A. & Khlebtsov, N. G. Determination of the size, concentration, and refractive index of silica nanoparticles from turbidity spectra. *Langmuir* **24**, 8964–8970 (2008).
37. Espiard, P. & Guyot, A. Poly(ethyl acrylate) latexes encapsulating nanoparticles of silica. 2. Grafting process onto silica. *Polymer* **36**, 4391–4395 (1995).
38. Castignolles, P., Graf, R., Parkinson, M., Wilhelm, M. & Gaborieau, M. Detection and quantification of branching in polyacrylates by size-exclusion chromatography (SEC) and melt-state 13C NMR spectroscopy. *Polymer* **50**, 2373–2383 (2009).
39. Berriot, J. et al. Filler–elastomer interaction in model filled rubbers, a 1H NMR study. *J. Non-Cryst. Solids* **307–310**, 719–724 (2002).
40. Zhang, M. et al. Liquid-crystal-elastomer-actuated reconfigurable microscale kirigami metastructures. *Adv. Mater.* **33**, 2008605 (2021).
41. Nandi, S. & Winter, H. H. Swelling behavior of partially cross-linked polymers: a ternary system. *Macromolecules* **38**, 4447–4455 (2005).
42. Frankær, S. M. G., Jensen, M. K., Bejenariu, A. G. & Skov, A. L. Investigation of the properties of fully reacted unstoichiometric polydimethylsiloxane networks and their extracted network fractions. *Rheol. Acta* **51**, 559–567 (2012).
43. Rivlin, R. S. & Thomas, A. G. Rupture of rubber. I. Characteristic energy for tearing. *J. Polym. Sci.* **10**, 291–318 (1953).

Acknowledgements This work was supported by the Materials Research Science and Engineering Centers (Grant DMR-2011754) and by the Air Force Office of Scientific Research (Grant FA9550-20-1-0397). J.S. was supported by a National Science Foundation Graduate Research Fellowship (Grant DGE1745303). J.K. was supported by the Kwanjeong Lee Chong Hwan Educational Foundation of Korea (Grant KEF-2017) and by the Korean Government (Electronics and Telecommunications Research Institute Grant 21YU1100). Silica nanoparticles used in this work were provided by Cabot Corporation. We acknowledge conversations on silica nanoparticles with A. Sanchez and D. Fomitchev at Cabot Corporation. We thank G. Zhang for measuring the sol and gel fractions.

Author contributions J.S. and J.K. designed the study and analysed the results. J.S. prepared samples and conducted monotonic and cyclic mechanical tests without cracks. J.K. measured crack growth and obtained images. J.S. and J.K. conducted demonstrations. Y.K. and Z.S. supervised the research. All authors wrote the manuscript.

Competing interests The authors declare no competing interests.

Additional information

Supplementary information The online version contains supplementary material available at https://doi.org/10.1038/s41586-023-06782-2.

Correspondence and requests for materials should be addressed to Yakov Kutsovsky or Zhigang Suo.

Peer review information *Nature* thanks the anonymous reviewers for their contribution to the peer review of this work. Peer reviewer reports are available.

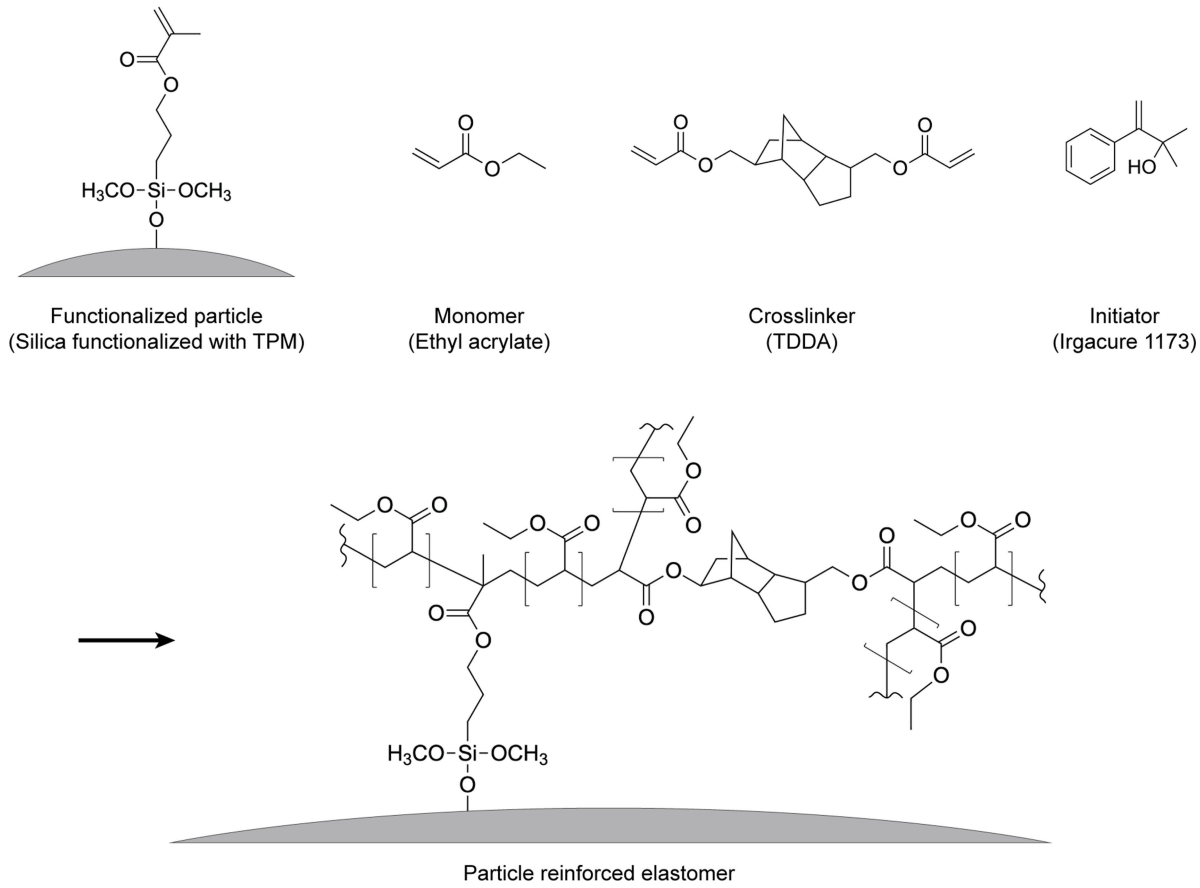

Extended Data Fig. 1 | Polymerization reaction of reinforced PEA elastomers. The molar coefficients of TDDA and Irgacure 1173 are normalized to 1 monomer of ethyl acrylate. The number of monomers between adjacent crosslinks after polymerization is estimated as $1/(2C)$.

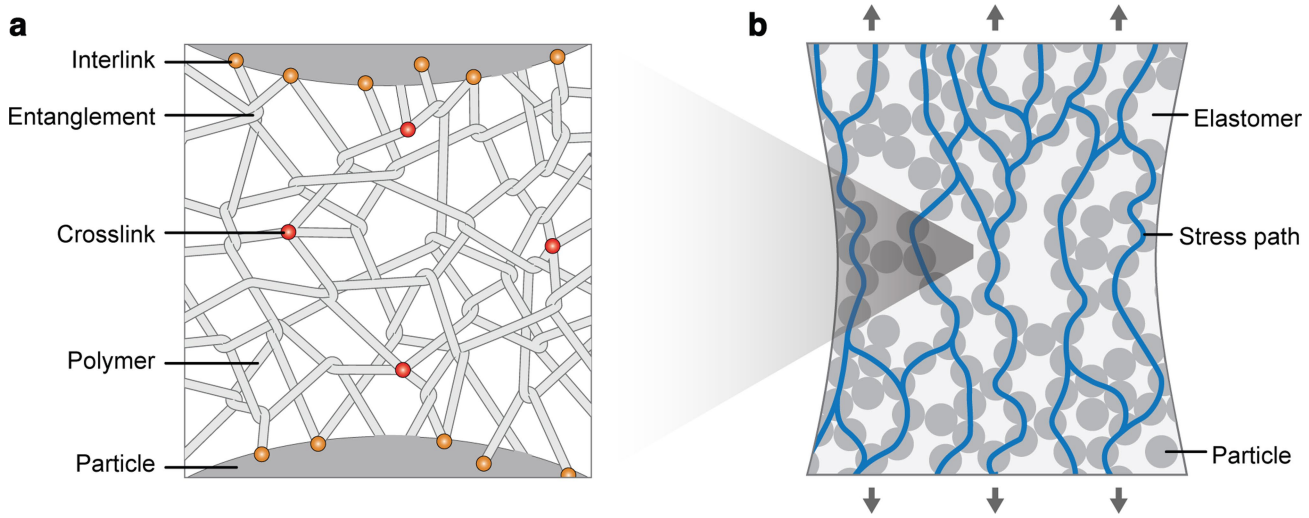

Extended Data Fig. 2 | Modulus is amplified by synergy of entangled polymer network and percolated particle network. (**a**) Long polymer chains form a network of sparse crosslinks and dense entanglements. Some of the polymer chains interlink with particles. (**b**) When particles form a percolated network, high stress transmits through the stiff particle network.

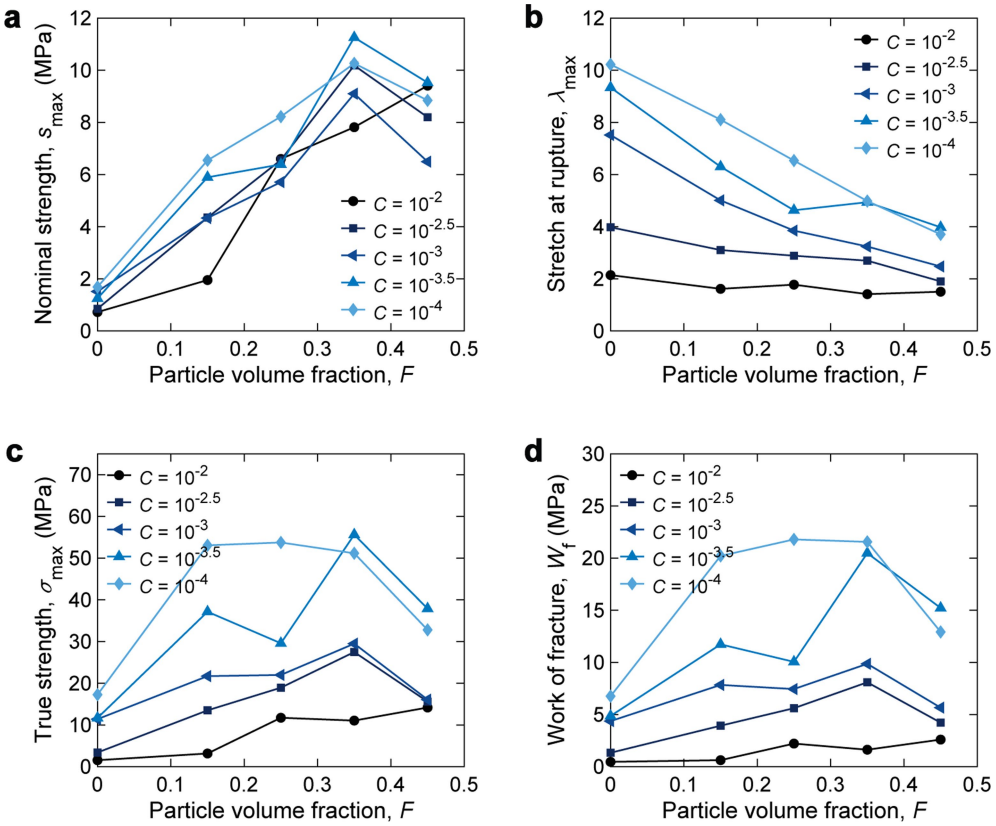

Extended Data Fig. 3 | Ultimate properties. (**a**) Nominal strength s_{max}, (**b**) stretch at rupture λ_{max}, (**c**) true strength σ_{max}, and (**d**) work of fracture W_f are plotted as functions of F with lines of constant C. All properties are measured at the point of rupture in the monotonic stress-stretch curves. s_{max} increases with increasing F, but changes with C weakly. By contrast, λ_{max} decreases with increasing F and increasing C. σ_{max} and W_f increase with decreasing C but do not show clear trends with F.

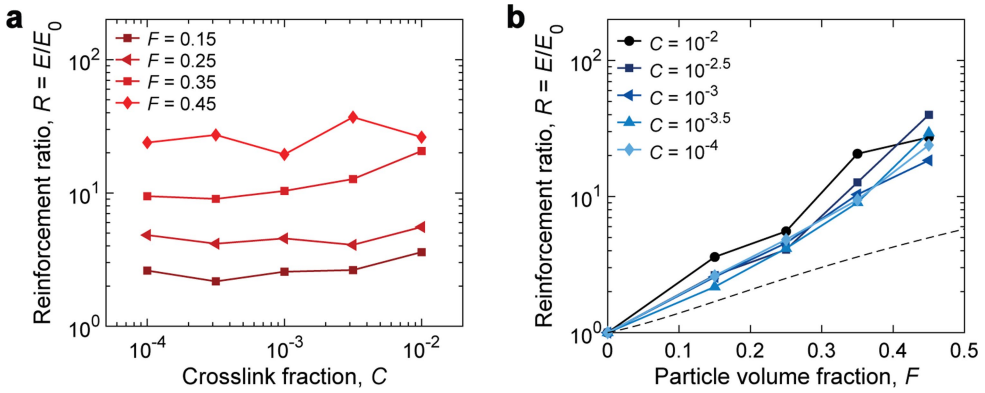

Extended Data Fig. 4 | Reinforcement ratio. The reinforcement ratio, $R = E/E_0$, is plotted as a function of (**a**) C with lines of constant F and (**b**) F with lines of constant C. The reinforcement ratio is not a function of C, but is a function of F. This suggests that the modulus of the composite takes the separable form $E(C, F) = R(F)E_0(C)$. The dashed line is the Guth-Gold solution.

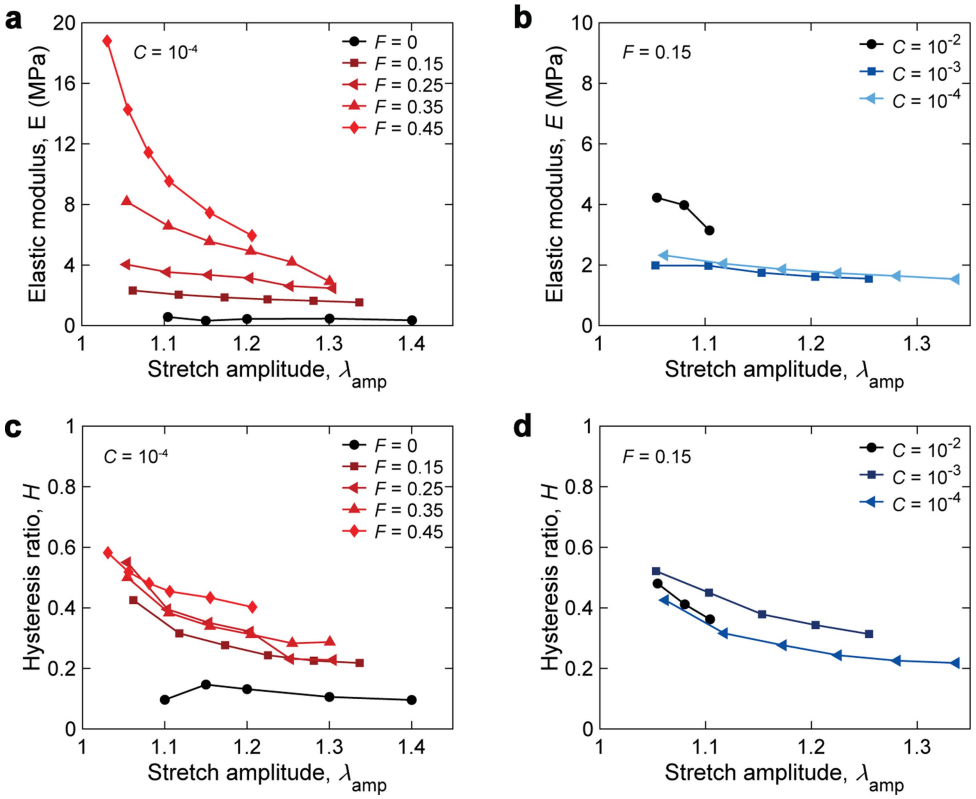

Extended Data Fig. 5 | Modulus and hysteresis ratio in cyclic stretch. Modulus E as a function of stretch amplitude λ_{amp} for (**a**) $C = 10^{-4}$ with various F and (**b**) $F = 0.15$ with various C. Hysteresis ratio H as a function of stretch amplitude λ_{amp} for (**a**) $C = 10^{-4}$ with various F and (**b**) $F = 0.15$ with various C. Both properties are calculated from the stress-stretch curves in the steady state. For composites of high F, the steady-state modulus decreases with increasing λ_{amp}. This behaviour suggests that particles form a percolated network and that large stretches induce changes in the microstructure, such as partial debonding between particles and polymers, breaking polymer chains, or formation of voids in the matrix. The modulus is insensitive to C when the polymers are highly entangled, which is consistent with the scaling $E = E_0 R$.

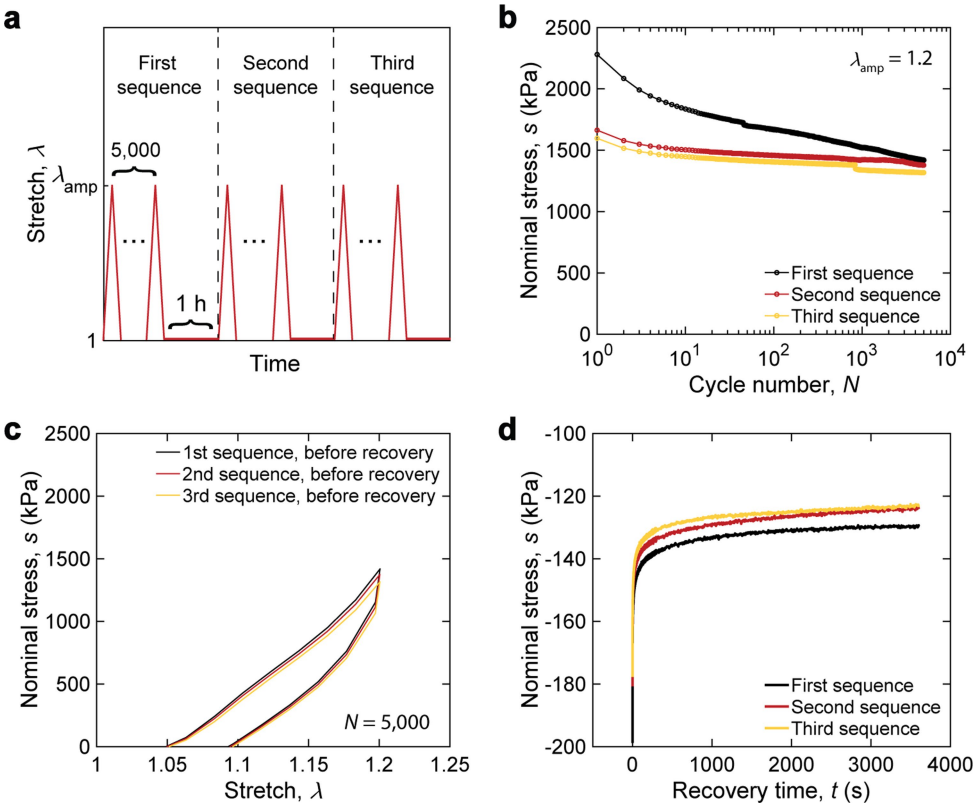

Extended Data Fig. 6 | Damage and recovery of composites. (**a**) Schematic of test. Using the pure shear geometry, a composite of $F = 0.45$ and $C = 10^{-4}$ is stretched for three sequences of $N = 5{,}000$ cycles and allowed to rest for 1 h. (**b**) The peak-force decays with cycles for all sequences, but more so in the first sequence. (**c**) The stress-stretch curves for the last cycle ($N = 5{,}000$) overlap for all sequences. (**d**) The stress during recovery relaxes with time at the same rate for all sequences.

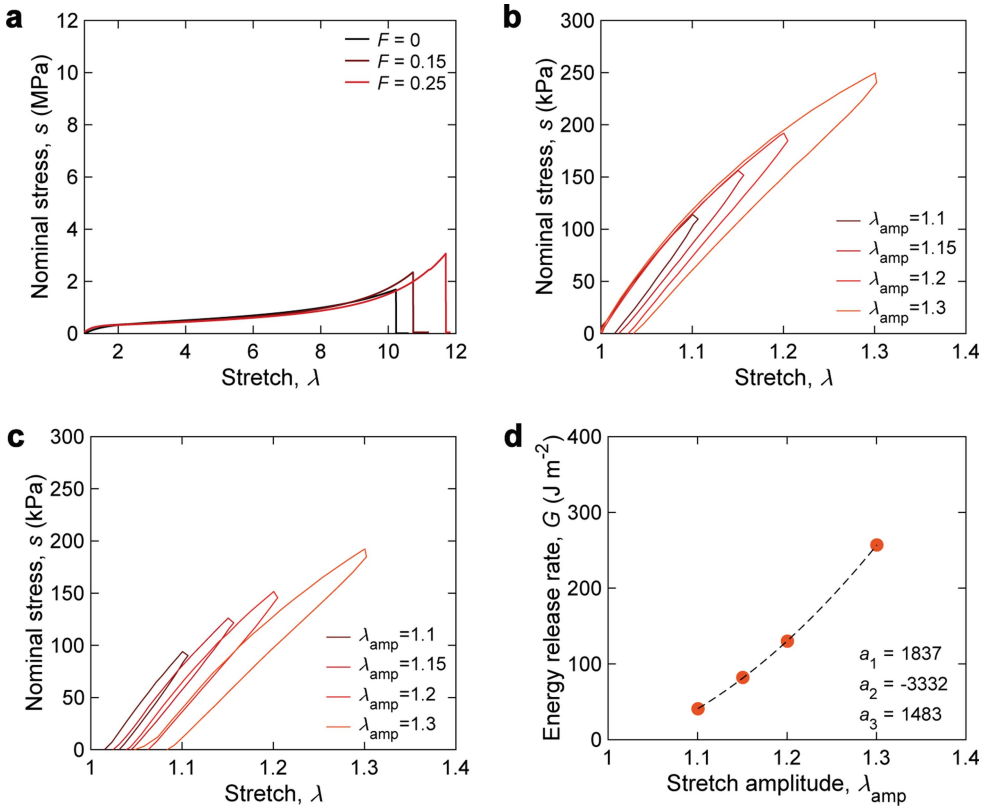

Extended Data Fig. 7 | Composite without covalent interlinks between polymers and particles. (**a**) Stress-stretch curves measured in uniaxial tension. Stress-stretch curves in pure shear (**b**) for the first load cycle and (**c**) after $N = 5{,}000$ cycles at various stretch amplitudes λ_{amp}. (**d**) Energy release rate G as a function of applied stretch λ_{amp} in the steady state, fit with a quadratic function $G = a_1\lambda_{amp}^2 + a_2\lambda_{amp} + a_3$. $C = 10^{-4}$ for all samples. $F = 0.15$ for samples in (**b**), (**c**), and (**d**).

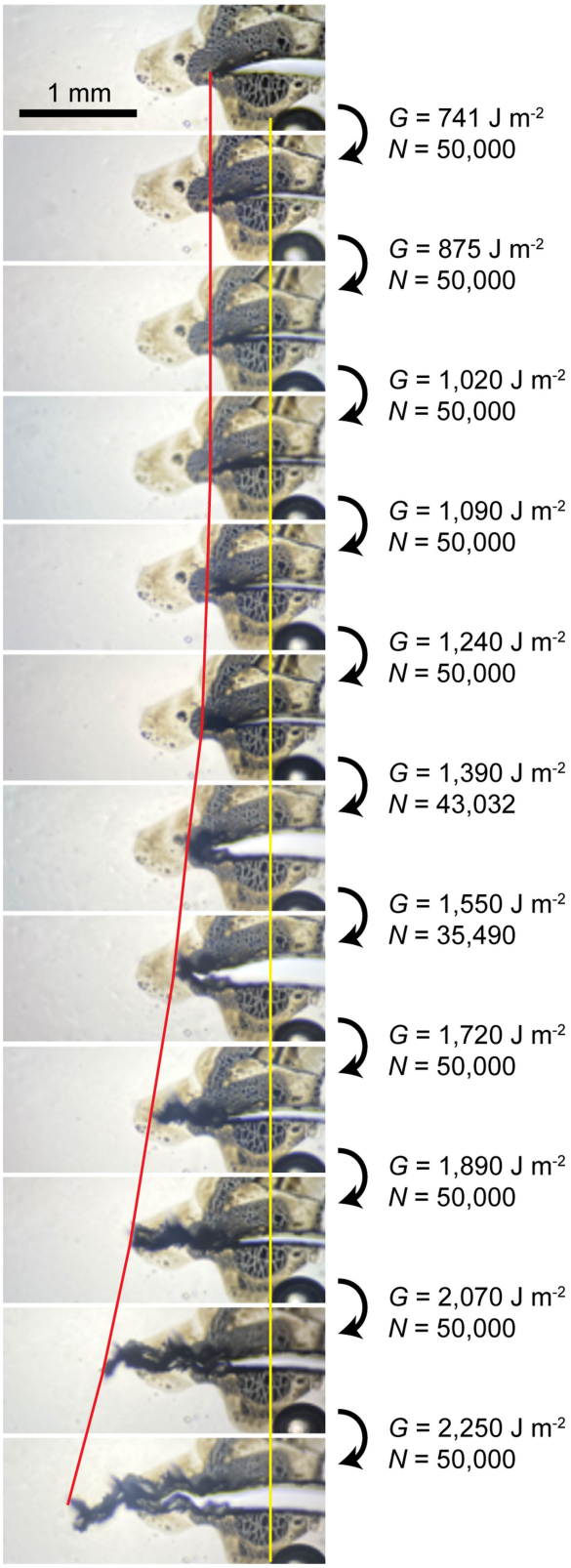

Extended Data Fig. 8 | Crack growth measurement for $F = 0.45$ and $C = 10^{-4}$. A crack is cut with scissors and marked with an ink pen. The sample is observed after N cycles of loading at steady-state energy release rate G. The yellow line is used to align the images, and the red line tracks the crack tip. The crack does not grow when $G \leq 1{,}020\ \mathrm{J\ m^{-2}}$.

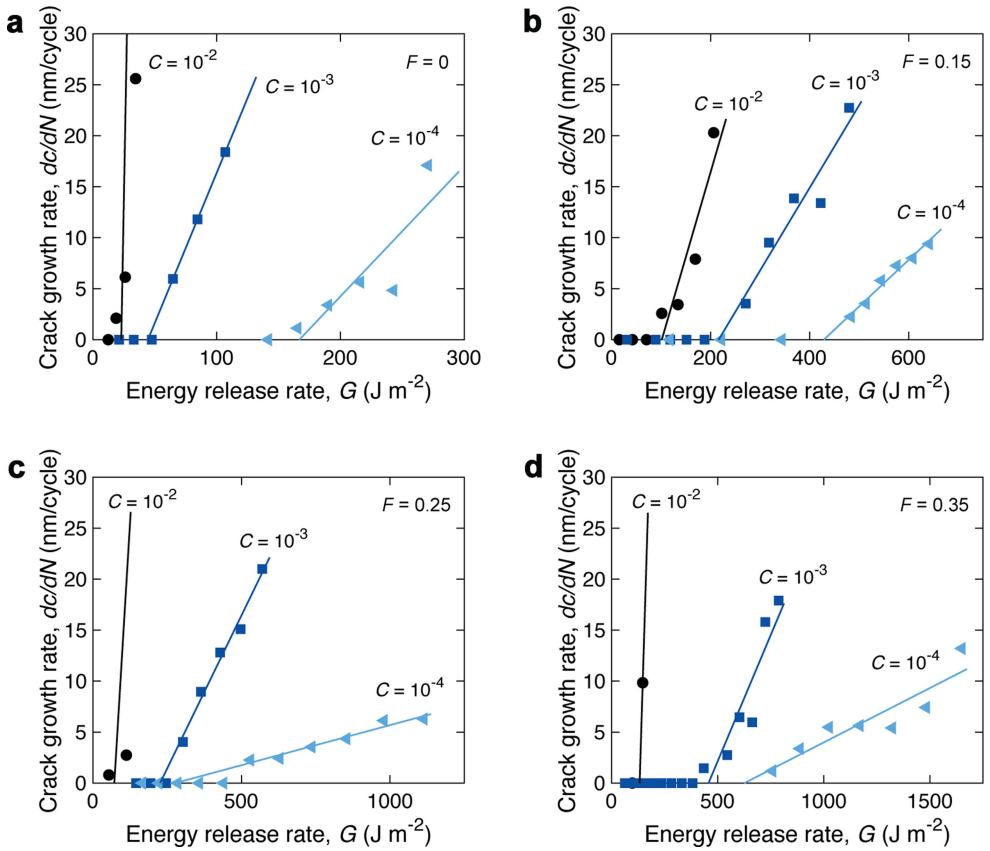

Extended Data Fig. 9 | Fatigue crack growth. Crack growth per cycle dc/dN as a function of energy release rate G for composites of (**a**) $F = 0$, (**b**) $F = 0.15$, (**c**) $F = 0.25$, and (**d**) $F = 0.35$ for various C.

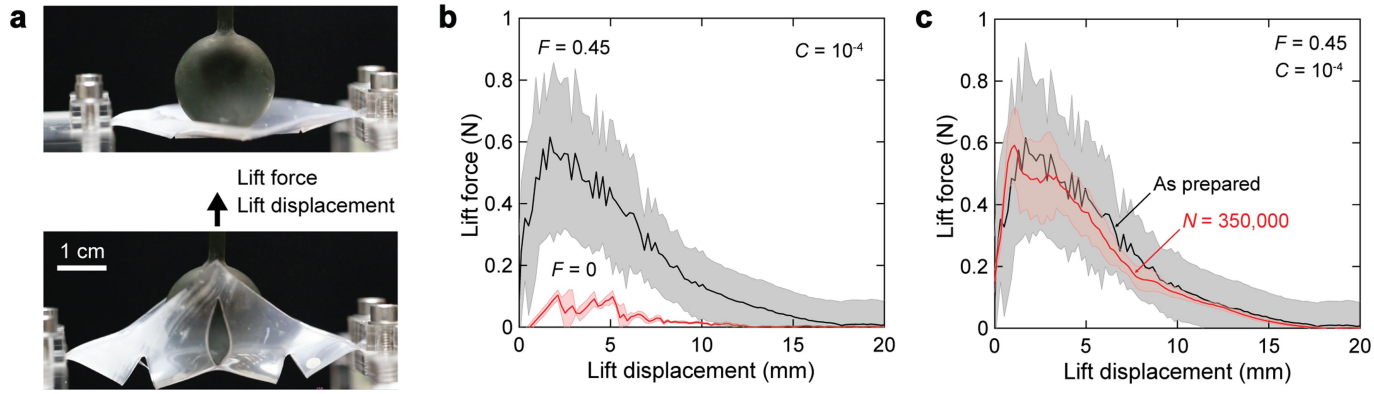

Extended Data Fig. 10 | Lift force of kirigami gripper. (**a**) When a sheet is pulled, it buckles and grips a sphere. The sphere is lifted at a constant velocity. (**b**) The lift force is measured as a function of lift displacement for grippers of $F = 0.45$ and $F = 0$ at fixed $C = 10^{-4}$. (**c**) A gripper of $F = 0.45$ and $C = 10^{-4}$ shows a lift force-displacement curve that is nearly unchanged after 350,000 cycles.